European Journal of Medicinal Chemistry 103 (2015) 600–614

Contents lists available at ScienceDirect

European Journal of Medicinal Chemistry

journal homepage: http://www.elsevier.com/locate/ejmech

Research paper

Ligand binding studies, preliminary structure–activity relationship and detailed mechanistic characterization of 1-phenyl-6,6-dimethyl-1,3,5-triazine-2,4-diamine derivatives as inhibitors of *Escherichia coli* dihydrofolate reductase

Bharath Srinivasan, Sam Tonddast-Navaei, Jeffrey Skolnick*

Center for the Study of Systems Biology, School of Biology, Georgia Institute of Technology, 950, Atlantic Drive, Atlanta, GA 30332, United States

ARTICLE INFO

Article history:
Received 21 May 2015
Received in revised form
29 July 2015
Accepted 9 August 2015
Available online 5 September 2015

Keywords:
Mechanistic characterization
Inhibition kinetics
Escherichia coli dihydrofolate reductase
QSAR
Drug discovery
2,4-Diamino-1,3,5-triazine
2,4-Diamino 1,2,4-triazine

ABSTRACT

Gram-negative bacteria are implicated in the causation of life-threatening hospital-acquired infections. They acquire rapid resistance to multiple drugs and available antibiotics. Hence, there is the need to discover new antibacterial agents with novel scaffolds. For the first time, this study explores the 1,3,5-triazine-2,4-diamine and 1,2,4-triazine-2,4-diamine group of compounds as potential inhibitors of *Escherichia coli* DHFR, a pivotal enzyme in the thymidine and purine synthesis pathway. Using differential scanning fluorimetry, DSF, fifteen compounds with various substitutions on either the 3rd or 4th positions on the benzene group of 6,6-dimethyl-1-(benzene)-1,3,5-triazine-2,4-diamine were shown to bind to the enzyme with varying affinities. Then, the dose dependence of inhibition by these compounds was determined. Preliminary quantitative structure–activity relationship analysis and docking studies implicate the alkyl linker group and the sulfonyl fluoride group in increasing the potency of inhibition. 4-[4-[3-(4,6-diamino-2,2-dimethyl-1,3,5-triazin-1-yl)phenyl]butyl]benzenesulfonyl fluoride (NSC120927), the best hit from the study and a molecule with no reported inhibition of *E. coli* DHFR, potently inhibits the enzyme with a K_i value of 42.50 ± 5.34 nM, followed by 4-[6-[4-(4,6-diamino-2,2-dimethyl-1,3,5-triazin-1-yl)phenyl]hexyl]benzenesulfonyl fluoride (NSC132279), with a K_i value of 100.9 ± 12.7 nM. Detailed kinetic characterization of the inhibition brought about by five small-molecule hits shows that these inhibitors bind to the dihydrofolate binding site with preferential binding to the NADPH-bound binary form of the enzyme. Furthermore, in search of novel diaminotriazine scaffolds, it is shown that lamotrigine, a 1,2,4-triazine-3,5-diamine and a sodium-ion channel blocker class of antiepileptic drug, also inhibits *E. coli* DHFR. This is the first comprehensive study on the binding and inhibition brought about by diaminotriazines of a gram-negative prokaryotic enzyme and provides valuable insights into the SAR as an aid to the discovery of novel antibiotics.

1. Introduction

The emergence and rapid dissemination of drug resistance in disease-causing gram-negative bacteria presents a challenge to the treatment of life-threatening hospital-acquired infections. This also poses a general threat to prevalent healthcare management practices by creating species resistant to all currently available antibacterial agents. There are several mechanisms by which gram negative bacteria acquire resistance to known drugs in the shortest possible time span. Most prominent among these are drug efflux pumps, acquisition of plasmids encoding antibiotic-resistance genes and acquisition of mutations in a biological target making it refractory to the action of the drug [1,2]. In fact, a survey of reported antibiotics of natural origin showed that among those compounds that showed activity against gram-positive bacteria, more than 90% lacked activity at a useful level against *Escherichia*

Abbreviations: *EcDHFR*, *Escherichia coli* dihydrofolate reductase; NADPH, nicotinamide adenine dinucleotide phosphate, reduced; H_2F, dihydrofolate; H_4F, tetrahydrofolate; QSAR, Quantitative Structure–Activity Relationship.

* Corresponding author.
E-mail addresses: bharath.srinivasan@biology.gatech.edu (B. Srinivasan), sam.tonddastnavaei@biology.gatech.edu (S. Tonddast-Navaei), skolnick@gatech.edu (J. Skolnick).

http://dx.doi.org/10.1016/j.ejmech.2015.08.021
0223-5234/

coli [3]. Given the alarming rise in instances of hospital-acquired infections by drug-resistant gram-negative bacteria [4–11], it becomes imperative to search for novel antibiotic agents against these organisms.

Dihydrofolate reductase, DHFR, is an important enzyme in the *de novo* pathway of purine and thymidine synthesis. Small-molecules targeting this enzyme have demonstrated utility as potential antibiotics [12]. However, this enzyme acquires rapid resistance to available antifolates. Several classes of compounds have been explored for their potential anti-folate activity. Predominant classes include diaminoquinazoline [13–18], diaminopyrimidine [19–22], diaminopteridine [23] and diaminotriazines [24].

Triazines are organic nitrogen containing heterocycles. They are classified into three different types based on the separation of the nitrogen atoms on the ring: 1,2,3-triazines, 1,2,4-triazines and 1,3,5-triazines. Among the three isomers, 1,3,5-triazine compounds are the best studied and are also known as symmetric triazines or *s*-triazines while 1,2,3-triazines are the least studied because of their poor stability [25]. 1,2,4-triazines have better solubility than 1,2,3-triazines and are comparatively better known, with the most prominent example being lamotrigine, a sodium-channel blocker class of anti-epileptic drug [26]. 1,2-dihydro-1,3,5-triazine (baker triazines) compounds are by far the best known with several studies exploring the potential of 2,4-diamino-1,3,5-triazines as inhibitors of eukaryotic DHFRs [24]. The most prominent example of the diaminotriazine group of compounds as DHFR inhibitors is the inhibition of *Plasmodium falciparum* DHFR by cycloguanil, a derivative of proguanil [27,28]. Detailed QSAR analysis of diaminotriazine derivatives has been carried out on DHFRs from several different organisms [29–39]. Recently, hybrids of triazines have also been demonstrated to show inhibitory activity on DHFRs [40,41].

However, most studies have focused on understanding the inhibitory effect of diaminotriazines on DHFRs from eukaryotic sources. Moreover, there is a total lack of kinetic characterization to understand their mechanism of DHFR inhibition. Knowledge of detailed kinetic mechanism is useful for designing effective drugs. One possible reason for the non-exploration of diaminotriazines as inhibitors of gram-negative bacterial DHFRs in general, and EcDHFR in particular, might stem from the consistently low affinities and poor inhibition by this class of molecules of prokaryotic DHFRs.

This study is the first attempt at detailed mechanistic characterization of diaminotriazine family of compounds by taking recourse to inhibition kinetics to assess their effect on EcDHFR. It also sheds valuable insights into the QSAR of 2,4-diamino-1,3,5-triazine inhibition of *E. coli* DHFR. Further, macromolecular docking studies provides valuable insights into the physical interactions that are likely responsible for conferring potency and specificity of the small-molecule/protein interaction. For the first time, we report two novel nanomolar inhibitors (NSC120927 and NSC132279) of a gram-negative prokaryotic DHFR from the 1,3,5-triazine-2,4-diamine class of molecules. This, combined with studies on the use of 1,2,4-triazine-3,5-diamine as novel scaffolds for *E. coli* DHFR inhibitors, opens up the possibility of exploring a new class of molecules that could potentially yield novel antibiotic candidates.

2. Results

2.1. Binding of 1,3,5-triazine-2,4-diamine analogs to EcDHFR

Binding of a small molecule ligand to the protein target of interest is a prerequisite for specific inhibition. Fifteen derivatives of 1,3,5-triazine-2,4-diamine were assessed for their ability to bind to the apo form of EcDHFR (Fig. 1). Differential scanning fluorimetry (DSF), a methodology relying on the increased protein stability conferred by small molecule binding as assessed by the environmentally-sensitive extrinsic fluorophore dye Sypro-Orange, was used to assess binding.

Fig 2 and Table 1 summarize the binding assay results. For ease of comprehension of results, molecules were classified into four different classes based on the chemical nature of substituents on the 1-phenyl-6,6-dimethyl-1,3,5-triazine-2,4-diamine group. Halide (NSC3074), methyl (NSC212229), methoxy (NSC19732) and ethoxy (NSC19745) substituents gave ΔT_m values ranging from ~10 °C to 13 °C (Fig 2A and Table 1). Nitrile (NSC115928) and dimethylamino (CHEMBL597262) substituents at R1 position and aminomethyl substituents (NSC168184) at the R2 position of 1-phenyl-6,6-dimethyl-1,3,5-triazine-2,4-diamine gave comparable ΔT_m values ranging from ~9 °C to 13 °C (Fig 2B and Table 1). However substitution of the aminomethyl group at the R1 position (NSC211137) drastically reduced binding as assessed by the magnitude of the thermal shift (~4 °C) (Fig 2B and Table 1). This might be because of unfavorable electrostatic interactions of this ligand with the apo form of the enzyme. Molecules having alkyl benzenesulfonyl fluoride (NSC120927 and NSC1332279), phenoxypropoxyphenyl (NSC133071), phenylbutyl (NSC132277) and fluorosulfonylphenylaminocarbonyl (NSC113909) substituents at either R2 or R1 position of 1-phenyl-6,6-dimethyl-1,3,5-triazine-2,4-diamine gave ΔT_m values ranging from ~11 °C to 23 °C (Fig. 2C and Table 1). Molecules in this class were by far the best binders as ranked by the apparent dissociation constants for all the ligands assessed in this study. It should be pointed out here that NSC132279 and NSC132277 were assessed at 10 μM concentrations rather than 500 μM, as was done for the other small-molecules. However, 2,4-dichlorophenylbutyl (NSC104129) substituent at R1 position gave a poor ΔT_m value of 5.8 °C (Fig 2C and Table 1). NSC117268, a compound containing 4-chlorophenyl and sulfonamide substitution at the R3 and R1 positions of 1,3,5-triazine-4,6-diamine group, gave a reasonable ΔT_m value of 7.6 °C (Fig 2D and Table 1). The results from binding analysis indicates that all 15 diaminotriazine small-molecules showed binding to *E. coli* DHFR to variable extents depending on the nature of the substituents.

2.2. Inhibition of EcDHFR by 1,3,5-triazine-2,4-diamine analogs

To further understand whether binding by these small molecules translates into inhibition, fourteen small molecules were tested for the dose-dependence of inhibition. NSC104129 and CHEMBL597262 were excluded from this analysis due to lack of sufficient quantities for inhibition studies. Fig 3A shows the experimental curves for dose-dependence of inhibition, and Table 1 summarizes the IC_{50} values for the 14 derivatives of 1,3,5-triazine-2,4-diamine tested. The apparent inhibition constants (K_{iapp}) were computed by fitting the curves to Morrison's quadratic equation (Fig 3B and Table 1). Once again, the values in Table 1 clearly show that derivatives with alkyl benzenesulfonyl fluoride (NSC120927 and NSC132279), phenoxypropoxyphenyl (NSC133071) and phenylbutyl (NSC132277) at either the R2 or R1 position of 1-phenyl-6,6-dimethyl-1,3,5-triazine-2,4-diamine are better inhibitors than the other small molecules employed in the study. The best hit was NSC120927 with a butyl benzenesulfonyl fluoride substitution at R2 position on 1-phenyl-6,6-dimethyl-1,3,5-triazine-2,4-diamine; it inhibited the enzyme with an IC_{50} and K_{iapp} value of ~1 μM and ~50 nM, respectively. The second best hit was NSC132279, a hexylbenzenesulfonyl fluoride substituted at R1 position, which showed an IC_{50} and K_{iapp} value of ~2 μM and ~93 nM, respectively.

However, the derivative with fluorosulfonylphenylamino carbonyl substitution (NSC113909), in spite of showing very tight

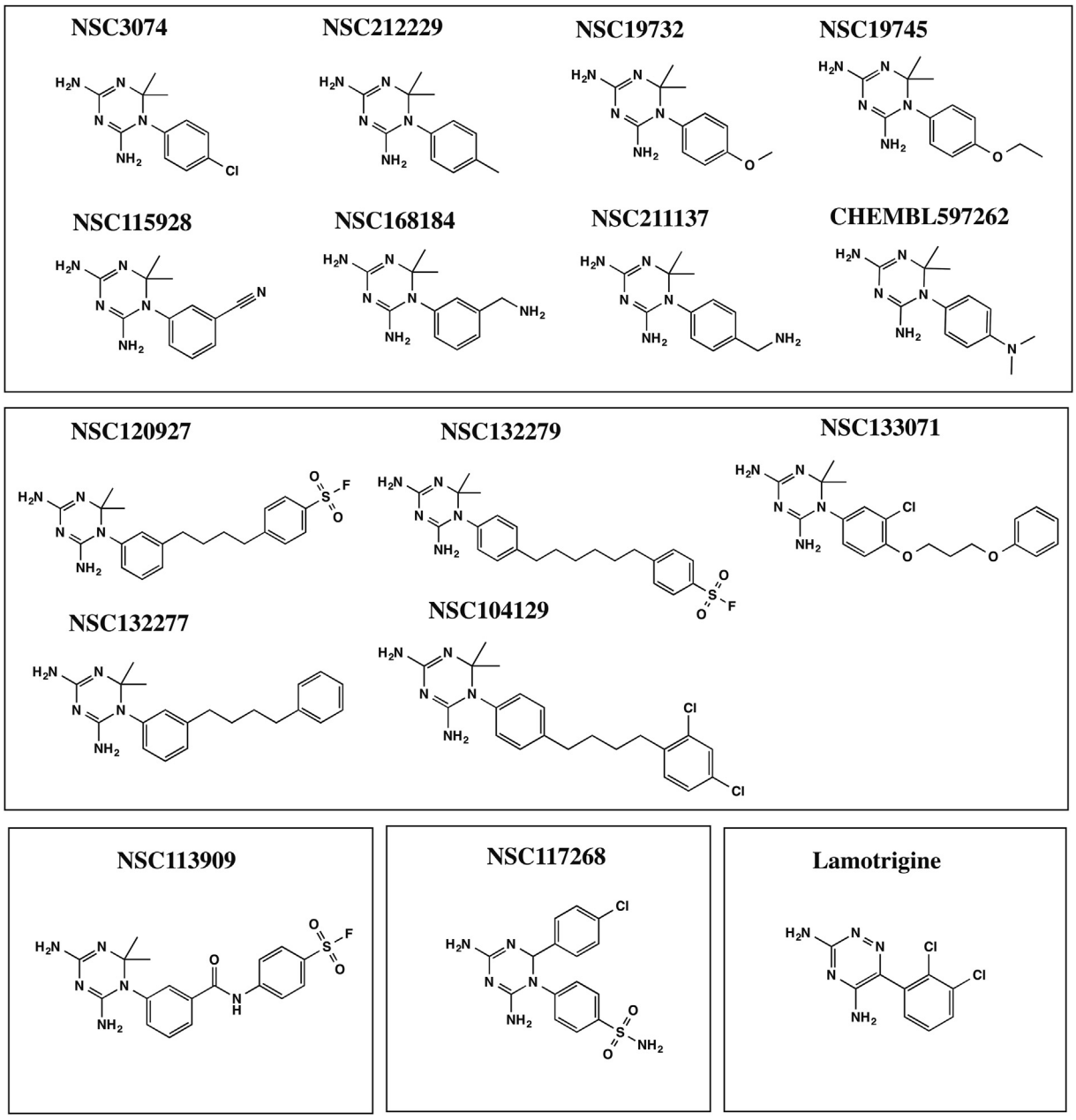

Fig. 1. Structures of diaminotriazines employed in this study. The structures were downloaded from PubChem with following PubChem CIDs: 3929273, 280860, 272645, 409219, 9049, 88868, 271921, 309795, 308877, 54606350, 280527, 274731, 419313, 3878, 1986. The molecules are binned into 5 different clusters based on a Tanimoto coefficient cutoff of 0.4.

binding as evident in a ΔT_m value of ~22 °C, poorly inhibited the enzyme with an IC_{50} and K_{iapp} value of ~63 μM and ~3 μM, respectively (Table 1). This might be because of the planarity of the peptide bond and partial charges introduced by the peptide group as a linker.

It should be noted that lamotrigine, a 1,2,4-triazine-3,5-diamine and a sodium-ion channel blocker class of antiepileptic drug, is also an inhibitor of *E. coli* DHFR inhibiting the enzyme with an IC_{50} and K_{iapp} of 348.9 ± 6.7 μM and 15.24 ± 2.78 μM, respectively (Table 1 and Fig 3). Weak inhibition by this compound could be ascribed to the lack of dimethyl hydrophobic substituents at the 6th position. Lamotrigine is substantially different structurally from the other 6,6-dimethyl-1,3,5-triazine-2,4-diamine derivatives employed in this study (Fig 1) and represents a novel scaffold that could be modified for design of new inhibitor molecules with activity against *E. coli DHFR*.

An important aspect to note is that the inhibition by this family of compounds does not conform to the slow-onset tight binding mechanism as evident in the linear time-course curves. It should be noted here that most other reported inhibitors of EcDHFR display slow-onset tight binding inhibition.

To further understand the relationship between the binding of these small-molecules to the apo form of the enzyme and inhibition assessed on the holo-enzyme, a scatter plot of $1/IC_{50}$ vs. ΔT_m was generated (Fig S1A). A Pearson correlation computed between the two parameters gave an R-value of 0.5774 and an R^2 of 0.33 indicating poor correlation. Lack of strong linear correlation between the magnitude of the thermal shift (hence binding)

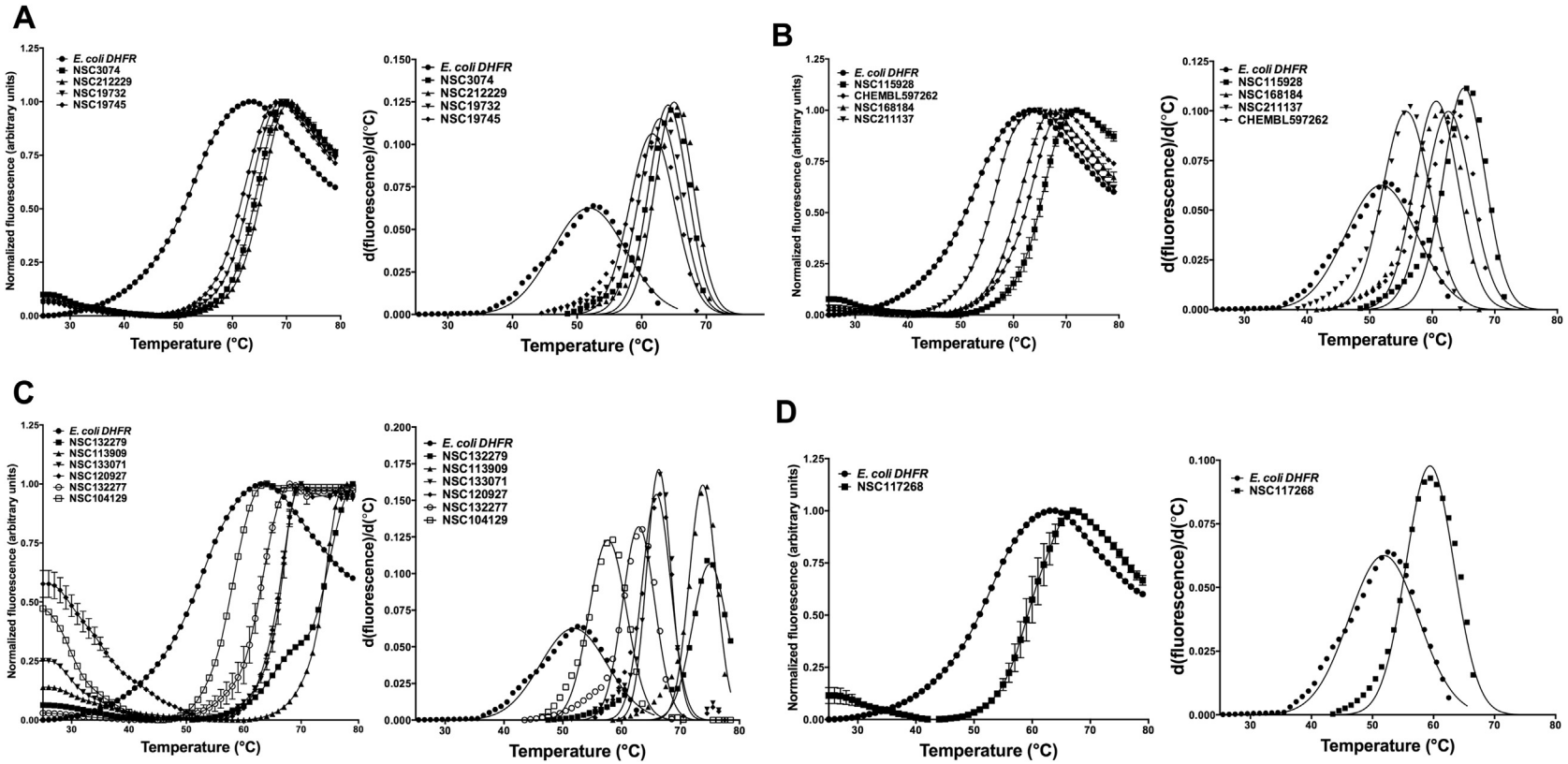

Fig. 2. Differential scanning fluorimetry, DSF, curves and their first derivatives for *E. coli* DHFR in the presence of 15 analogs of 1,3,5-triazine-2,4-diamine. (A) DSF curves for halide, methyl, methoxy and ethoxy substituents at the R1 position of 1-phenyl-6,6-dimethyl-1,3,5-triazine-2,4-diamine. (B) DSF curves for nitrile, dimethylamino and aminomethyl substituents at either R1 or R2 position of 1-phenyl-6,6-dimethyl-1,3,5-triazine-2,4-diamine. (C) DSF curves for alkyl benzenesulfonyl fluoride, phenoxypropoxyphenyl, phenylbutyl, 2,4-dichlorophenylbutyl and fluorosulfonylphenylaminocarbonyl substituents at either R1 or R2 position of 1-phenyl-6,6-dimethyl-1,3,5-triazine-2,4-diamine. Note that this class of molecules showed the largest thermal shifts. (D) DSF curve for 4-chlorophenyl and sulfonamide substitution at the R1 and R3 position of 1-phenyl-1,3,5-triazine-4,6-diamine. The y-axis in primary unfolding curves represents normalized fluorescence and the x-axis shows the temperature in degrees Celsius. The inhibitors were kept fixed at 500 μM except NSC132277 and NSC132299, which were done at 10 μM concentration. Right panel in each plot shows the Gaussian fit of first-derivative for curves from left panel. Note that the molecules NSC117268, NSC133071, NSC168184, NSC104129, CHEMBL597262 and NSC333873 were also independently picked by the virtual ligand screening algorithm, PoLi.

Table 1
Summary of binding and inhibition parameters for diaminotriazine derivatives employed in this study.[b]

Root structure$_1$ 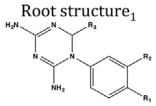

Chem ID	Position	Substitution	Binding and inhibition potency				
			ΔT_m (°C)[c]	K_{Dapp} (μM)[d]	ClogP[g]	IC-50 (μM)	$K_{i\ app}$[a] (μM)
NSC120927	R2, R3	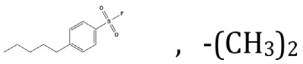	14.05	6.93	3.8490	1.15 ± 0.37	0.0497 ± 0.004
NSC132279[f]	R1, R3	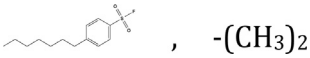	23.13	0.01	4.9070	1.84 ± 0.13	0.0926 ± 0.010
NSC132277[f]	R2, R3	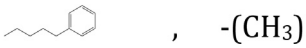	11.04	0.34	3.6860	7.59 ± 0.24	0.3591 ± 0.032
NSC133071	R1, R2, R3	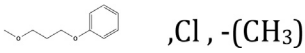	14.45	6.16	3.1958	18.45 ± 0.33	0.8802 ± 0.075
NSC104129[e]	R1, R3	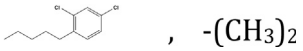	5.8	82.55	5.1120	ND	ND
NSC115928	R2, R3		13.26	8.74	0.0115	20.19 ± 0.56	0.958 ± 0.06
NSC3074	R1, R3	$-Cl$, $-(CH_3)_2$	12.25	11.77	1.0658	20.91 ± 1.01	1.02 ± 0.12
NSC212229	R1, R3	$-CH_3$, $-(CH_3)_2$	13.17	9.32	0.6810	32.27 ± 0.83	1.55 ± 0.11
NSC19732	R1, R3	$-O-CH_3$, $-(CH_3)_2$	10.97	17.23	0.4547	89.10 ± 2.75	4.02 ± 0.46
CHEMBL597262[e]	R1, R3	$-N(CH_3)_2$, $-(CH_3)_2$	10.73	18.51	0.6520	ND	ND
NSC19745	R1, R3	$-O-CH_2-CH_3$, $-(CH_3)_2$	9.79	24.53	0.9837	262.7 ± 6.68	11.16 ± 1.14
NSC168184	R2, R3	$-CH_2-NH_2$, $-(CH_3)_2$	8.79	33.16	−0.8660	478.4 ± 7.28	20.22 ± 3.10
NSC211137	R1, R3	CH_2-NH_2, $-(CH_3)_2$	3.99	144.54	−0.866	721.6 ± 6.65	39.30 ± 4.05
NSC113909	R2, R3		21.92	0.73	1.8274	62.83 ± 2.13	2.89 ± 0.35
NSC117268	R1, R3	$SO_2(NH_2)$ 	7.57	48.01	0.4315	1548 ± 40	105.0 ± 13.51
Lamotrigine[b]		NA	ND	ND	2.5343	348.9 ± 6.7	15.24 ± 2.78

[a] The K_{iapp} values are computed by fitting the dose-dependence inhibition curves to Morrison equation.
[b] All structures except lamotrigine.
[c] Thermal shift reported are at 500 μM ligand concentration in the absence of NADPH. The Tm for protein alone curve is 51.9 °C.
[d] Approximate dissociation constant computed from the magnitude of thermal shift.
[e] No inhibition done.
[f] No signal seen at 500 μM and hence values reported for 10 μM.
[g] Values computed by ChemBioDraw 14.0. ND, not determined. NA, not applicable.

and inhibition indicates that there might be substantial differences between the mode of binding and inhibition. Moreover, since binding was assessed in the absence of NADPH, it is possible that occupancy of the NADPH binding pocket may change the charge distribution in the diaminotriazine small-molecule binding pocket.

2.3. Quantitative structure–activity relationship analysis and macromolecular docking

To quantitatively understand the inhibition brought about the diaminotriazine series of compounds studied and to increase the predictive value of the current study in its ability to find more potent inhibitors, a QSAR analysis was carried out. Various physicochemical parameters (like hydrogen bond donors, hydrogen bond acceptors, total polar surface area, geometrical shape coefficient etc) of the molecules were computed employing OpenBabel, Joelib and ChemmineR descriptors. Most of the parameters, when individually assessed, showed no correlation with inhibition potency and a representative scatter plot for tPSA depicting this lack of correlation is shown in Fig S1B. However, inhibition by these molecules showed good correlation to both atomistic (LogP) and fragment-based partition coefficient (CLogP) (Fig S1C and S1D), whereby increasing the hydrophobicity of a compound led to increased inhibition. The equations defining the relationship between the partition coefficients of the small-molecules and the respective inhibition constants are shown in the figure along with the regression measure. This result is in broad agreement with already reported QSAR analysis for DHFRs from eukaryotic sources which had indicated that hydrophobic triazines are particularly effective against *Pneumocystis carinii* DHFR [34] and mammalian DHFRs [31]. This similarity in QSAR behavior is in spite of the low sequence similarity shared by the prokaryotic and eukaryotic DHFRs.

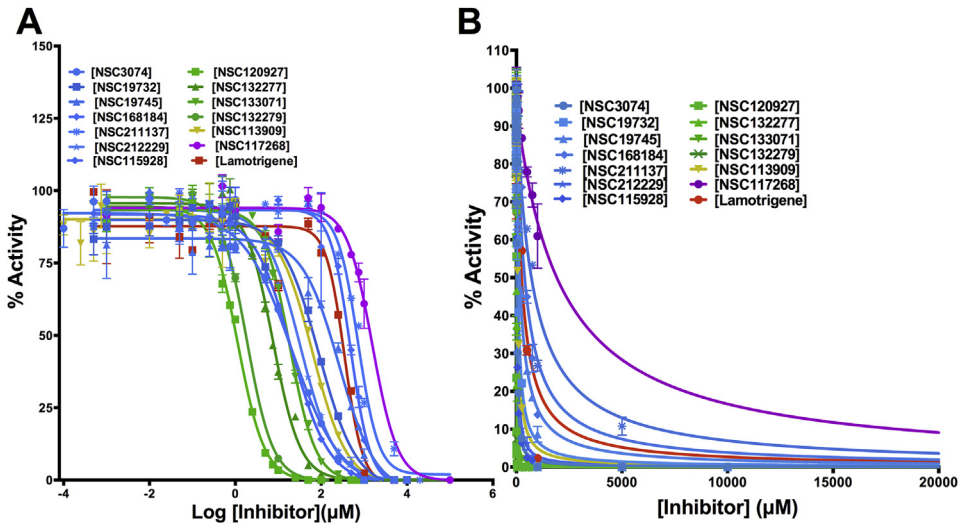

Fig. 3. Dose-dependent inhibition of *E. coli* DHFR by analogs of 1,3,5-triazine-2,4-diamine. (A) IC_{50} determination of 14 compounds. (B) Fit of the experimental dose–response curves to Morrison's equation to compute the K_{iapp} for various inhibitors of *E. coli* DHFR. Curves showing inhibition by derivatives having halide, methyl, methoxy, ethoxy, nitrile, dimethylamino and aminomethyl substituents at either the R1 or R2 position of 1-phenyl-6,6-dimethyl-1,3,5-triazine-2,4-diamine are shown in blue; derivatives having alkyl benzenesulfonyl fluoride, phenoxypropoxyphenyl and phenylbutyl at either R1 or R2 position of 1-phenyl-6,6-dimethyl-1,3,5-triazine-2,4-diamine are shown in green; derivative having fluorosulfonylphenylaminocarbonyl at R2 position of 1-phenyl-6,6-dimethyl-1,3,5-triazine-2,4-diamine is shown in gold; derivative having a 4-chlorophenyl and benzenesulfonamide substitution at the R1 and R3 position of 1-phenyl-1,3,5-triazine-4,6-diamine are shown in pink; Lamotrigine, a 6-(2,3-dichlorophenyl)-1,2,4-triazine-3,5-the diamine is shown in red. All activities are expressed as percentage activity. The numbered notations for the various inhibitor molecules represent NSC numbers. (For interpretation of the references to colour in this figure legend, the reader is referred to the web version of this article.)

To perform a more definitive QSAR, a genetic algorithm (GA)-based heuristic methodology was employed for selection of significant variables that influences inhibition [42]. Genetic algorithms are a subclass of evolutionary algorithms (EA) that are employed for generating solutions to optimization problems involving multiple variables employing the principles of natural evolution like inheritance, mutation, crossover and selection. The best solution with good statistics of fit is given below

$$\begin{aligned}\text{Log } 1/K_{\text{iapp}} &= 0.90(\pm 0.79) - 0.61(\pm 0.22)\text{bonds} \\ &\quad + 0.80(\pm 0.40)\text{nF} - 1.2(\pm 0.26)\text{HBD} \\ &\quad + 0.6(\pm 0.22)\text{atoms}; \\ \text{R} &= 0.922\end{aligned}$$

“bonds” indicate the number of single bonds, “nF” indicates the number of fluorine atoms and “HBD” indicates hydrogen-bonding donors.

This result, along with the correlation that LogP score showed, indicates that the number of fluorine atoms, hydrogen bonding donors and LogPs contribute to better fits. Thus, the presence of an alkyl benzene group in general, and the alkyl benzenesulfonyl fluoride group in particular, has a major influence in determining inhibition potency. This provides vital clues about the type of modifications that might be desirable on the small-molecules to increase their potency of inhibition.

To understand the physical basis for inhibitor discrimination, template-based macromolecular rigid body docking was carried out. The conformation of folate in complex with DHFR [43] was used as reference for docking the small molecules inside DHFR's binding site. To understand the procedure, it is helpful to describe the interaction of folate with DHFR in more detail, as shown in Fig. 4A. The folate molecule can be broken into three fragments based on the interaction each fragment has with DHFR's active-site pocket and the pocket's neighboring residues; (a) The 2-amino-4-oxo-1,4-dihydropteridin group interacts with the active-site pocket residues of DHFR, (b) The methylaminobenzoyl group in the middle of folate is in contact with four hydrophobic amino acids (Leu28, Phe31, Ile50 and Leu54) and finally (c) The polar and negatively charged glutamic acid tail fragment of the folate interacts with the positive triad of Lys32, Arg52 and Arg57 located at the entrance of the binding site.

After aligning different conformations of the various small molecules to folate (see Methods section), the best alignment for each case was chosen based on the highest combined shape and chemical similarity scores (Table 2) given by LIGSIFT [44]. All five small-molecules share the diaminotriazine group, which is aligned to the 2-amino-4-oxo-1,4-dihydropteridin group of folate and ends up interacting with the binding site amino acids (Fig. 4 B–F). Therefore, the differential affinity of these molecules could be due to the dissimilarity in the other regions that we next explain in more detail. The molecule that shows good binding and most potent inhibition, NSC120927 (Fig. 4B), shows the best scores for shape and chemical similarity when compared to the rest of the molecules, with significant p-values as shown in Table 2. In this case, the sulfonyl fluoride group aligns to the tail fragment of folate allowing it to preserve the favorable interaction with the triad of positive residues located at the entrance of the binding site. Also, the central hydrophobic fragment of NSC120927 (two aromatic rings linked by four carbons) aligns to the middle fragment of folate and can interact strongly with the hydrophobic patch made of Leu28, Phe31, Ile50 and Leu54.

The second best molecule, NSC132279 (Fig. 4C), has almost the same structure as the first with a minor difference. Now, the two aromatic rings are connected with a longer linker (six carbons) making it slightly harder for it to fit within the pocket (reflected in the lower shape and chemical similarity scores in Table 2) and preserve the interaction with the hydrophobic patch. Therefore, the strong binding and inhibition by NSC120927 and NSC132279 can be ascribed to possible charged group interactions formed by the negative groups on the ligands with the apo protein target as well as their interaction with the hydrophobic patch. Hydrogen bonding of the charged moiety is possible; as evident in Fig S2, which shows that the distances and angles of the charged portion of NSC120927

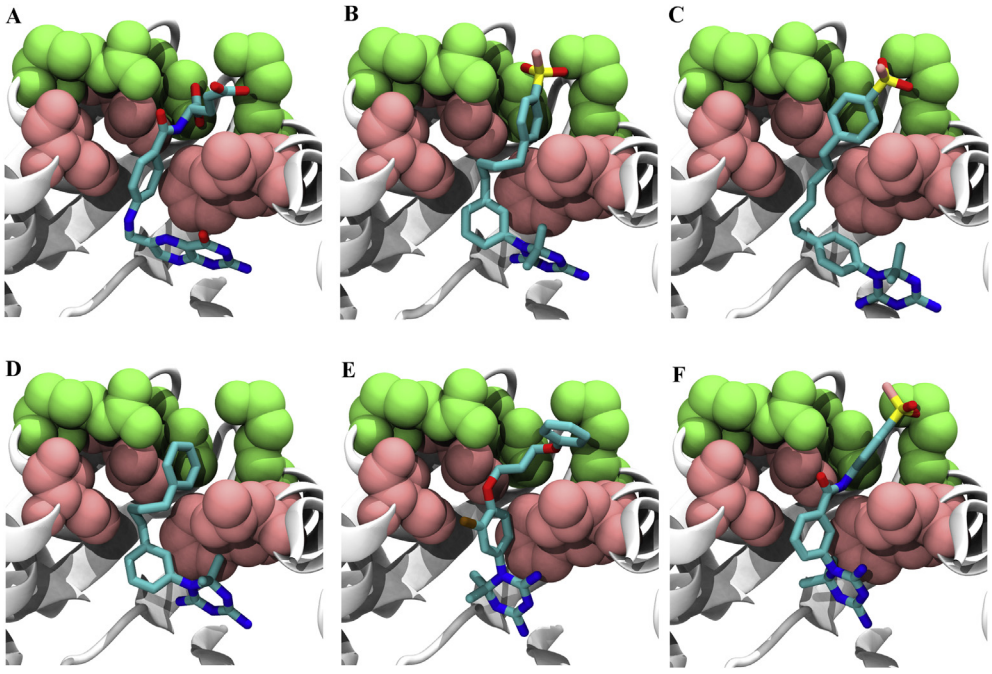

Fig. 4. Template-based docking of the best hits from the study (A) Folate (B) NSC120927 (C) NSC132279 (D) NSC132277 (E) NSC133071 (F) NSC113909. The positive charged ring located at the entrance of the pocket (Lys 32, Arg52 and Arg57) is shown in green van der Waals representation. DHFR is shown in a white cartoon representation. The hydrophobic ring (Leu28, Phe31, Ile50 and Leu54) is shown in a pink van der Waals representation. Ligands are presented in licorice format showing the heavy atoms: carbon (cyan), nitrogen (blue), oxygen (red), sulfur (yellow), fluorine (pink), chlorine (ochre). The figures were rendered using Tachyon [64] and VMD [65] was used for visualization. (For interpretation of the references to colour in this figure legend, the reader is referred to the web version of this article.)

Table 2
The best alignment scores and the corresponding P-value for each of the predicted molecules.

Name	ShapeSim[a]	P-value	ChemSim[b]	P-value
NSC120927	0.617	3.96×10^{-2}	0.460	6.78×10^{-2}
NSC132279	0.599	7.58×10^{-2}	0.421	1.85×10^{-1}
NSC132277	0.634	2.37×10^{-2}	0.447	1.05×10^{-1}
NSC133071[c]	0.564	7.87×10^{-2}	0.329	7.03×10^{-1}
NSC113909	0.596	8.34×10^{-2}	0.461	6.98×10^{-2}

[a] Shape-similarity score calculated by LIGSIFT.
[b] Chemical-similarity score calculated by LIGSIFT.
[c] This case was the only one with no significant score when considering both shape and chemistry mode of LIGSIFT for the alignment, therefore only shape mode was used for this case. For the other cases shape + chemistry mode of LIGSIFT was used to generate the alignments.

are compatible with formation of moderate to strong hydrogen bonds [45,46]. As depicted in the figure, the angles of the predicted hydrogen bonds are between 145 and 160° and the distances are between 1.56 and 2.80 Å. This observation is in agreement with obtained QSAR results that selected "hydrogen-bonding donor" as a possible variable that determines efficacy of inhibition.

The third molecule, NSC132277 (Fig. 4D), has the same structure as NSC120927 but lacks the sulfonyl fluoride group. Hence, it loses favorable interactions with the positively charged ring, and thus, has lower affinity (Table 1). The next molecule, NSC133071 (Fig. 4E), also lacks the sulfonyl fluoride group of NSC120927. Additionally, chlorine is introduced in one of the aromatic rings, and the chlorophenoxypropoxy linker between the two rings has two oxygen atoms rather than a phenyl alkyl linker (Fig 1). The docking pose of NSC133071 shows that the chlorine and one of the two oxygen atoms are in the vicinity of the hydrophobic patch, therefore resulting in unfavorable interactions and lower binding affinity.

NSC113909 is a unique molecule that shows good binding, but poor inhibition of *E. coli* DHFR. NSC113909 (Fig. 4F) shows higher shape similarity than NSC133071 to folate and the chemical similarity is same as that of the best molecule (NSC120927). The disparity between binding and inhibition could be explained by the fact that the charged interactions made by the sulfonyl fluoride group is preserved while the peptide bond as linker between two aromatic rings is unfavorable for bringing about effective inhibition. We suggest that the peptide bond locks the molecule in fewer conformations and reduces its degrees of freedom, thereby making it harder for it to access the binding site due to steric effects in the NADPH-bound holo enzyme. Moreover, burying the charges on the peptide moiety of NSC113909 in the NADPH-bound holo protein might impose an energetic cost making it a weaker inhibitor.

In summary, preliminary QSAR and macromolecular rigid-body docking studies indicates that the length of the alkyl linker and the sulfonyl fluoride group play pivotal roles in determining the potency of inhibition.

2.4. 1,3,5-Triazine-2,4-diamine analogs as competitive inhibitors of H_2F binding

To further understand the inhibition shown by derivatives of 1,3,5-triazine-2,4-diamines, we resorted to detailed inhibition kinetics. The top four inhibitors showing the lowest K_{iapp} values, indicating highest affinities, were selected to understand the mechanism of inhibition. To better understand the mechanism, the analysis was split into inhibition brought about by alkyl benzenesulfonyl fluoride substituents at either R2 (NSC120927) or R1 (NSC132279) position of 1-phenyl-6,6-dimethyl-1,3,5-triazine-2,4-diamine ring and those shown by phenoxypropoxyphenyl (NSC133071) and phenylbutyl (NSC132277) substituents.

Substrate dihydrofolate (H_2F) was titrated at several fixed concentrations of NSC120927 and NSC132279, and the resulting curves from the experiment were globally fit to models for the various

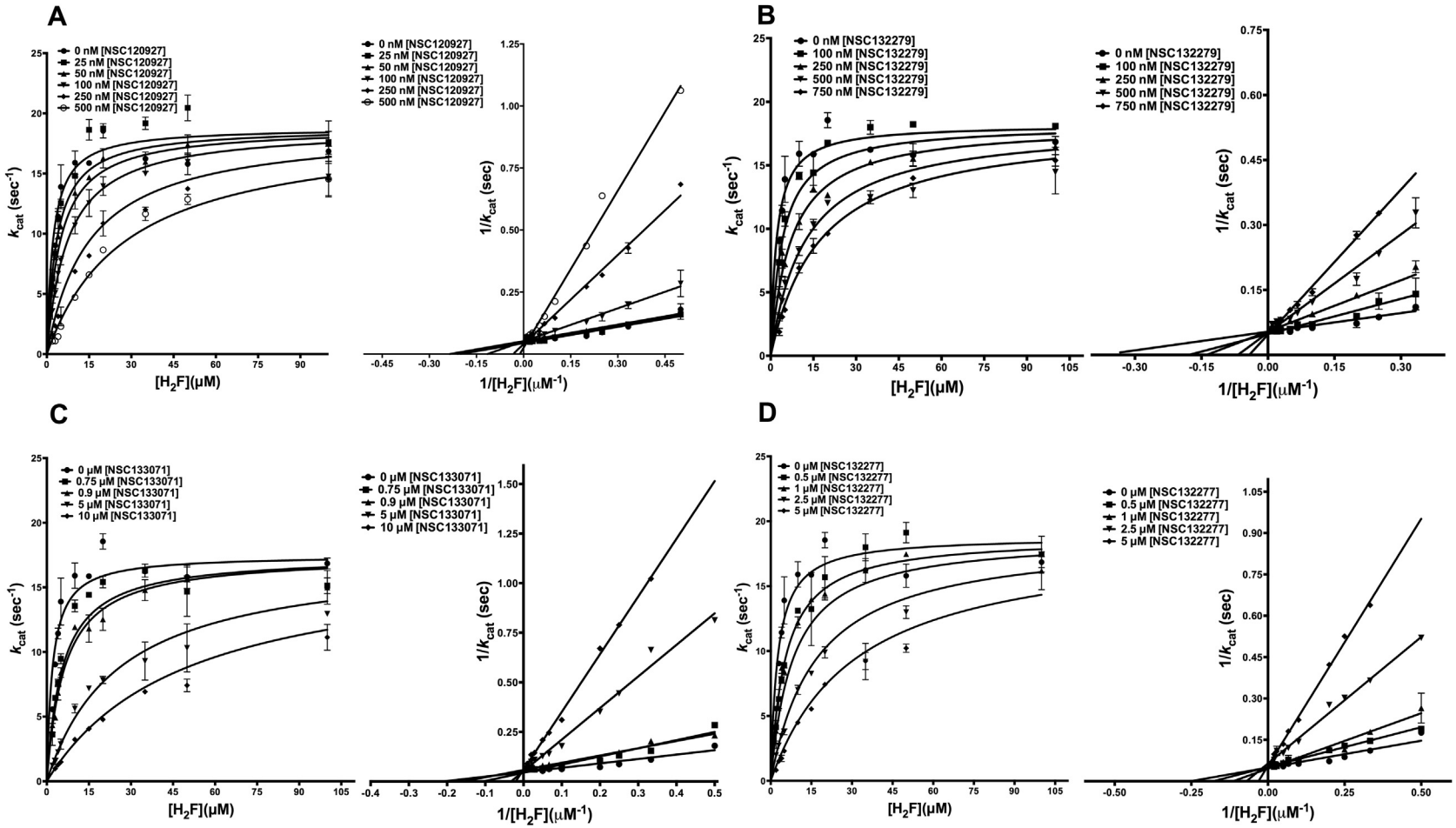

Fig. 5. Competition experiments of NSC120927, NSC132279, NSC133071 and NSC132277 against substrate H_2F for *E. coli* DHFR. The figure shows the fit of the primary data to the competitive inhibition model and double reciprocal Lineweaver–Burk plot for H_2F titration at several fixed concentrations of (A) NSC120927 (B) NSC132279. (C) NSC133071 and (D) NSC132277. The y-axis shows the k_{cat} and k_{cat}^{-1} value and the x-axis shows the [H_2F] and 1/[H_2F] values for the primary and LB plot, respectively. The experimental data points were fit to the respective models using the non-linear curve-fitting algorithm of GraphPad Prism v 6.0e.

Table 3
Parameters from inhibition kinetics of *E. coli* DHFR.

Inhibitors	Substrate	Inhibition	$K_i/\alpha K_i$ (nM)[a]
NSC120927	H_2F	Competitive	42.50 ± 5.34
	NADPH	Uncompetitive	946.4 ± 62.3
NSC132279	H_2F	Competitive	100.9 ± 12.7
	NADPH	Uncompetitive	2019 ± 155
NSC132277	H_2F	Competitive	394.3 ± 58.4
	NADPH	Uncompetitive	7432 ± 375
NSC133071	H_2F	Competitive	430 ± 53.8
	NADPH	Uncompetitive	12,300 ± 793
NSC113909	H_2F	Competitive	3816.0 ± 434.0
	NADPH	Uncompetitive	62,240 ± 3557

[a] The K_i is reported for competitive inhibition while αK_i is reported for uncompetitive inhibition.

types of inhibition. A sum-of-square F-test was performed to validate the non-linear fits. Both the curves for NSC120927 and NSC132279 showed the best fit to the model for competitive inhibition (Figs. 5A and 5B) yielding a K_i, the equilibrium dissociation constant for the competitive inhibitor, of 42.50 ± 5.34 nM and 100.9 ± 12.7 nM, respectively (Table 3). Further, for visual understanding, the data were transformed and plotted as the double-reciprocal Lineweaver–Burk plot, LB. The right hand panels in Fig. 5A and B show the lines of the LB-plot intersecting on the ordinate. This is further indicative of competitive displacement of substrate dihydrofolate at saturating NADPH by NSC120927 and NSC132279, whereby increasing concentration of the inhibitors decreases the affinity for H_2F without unduly affecting the maximal velocity of the reaction. It should be pointed out that for NSC120927 and NSC132279, the K_i values are ~27-fold and ~18-fold lower than the obtained IC_{50} values for the respective ligands. The above data is conclusive about the inhibitors binding to the same site as the substrate H_2F, competing with the substrate for high-affinity interactions with the enzyme. This competitive displacement can be ascribed to the diaminotriazine group that shares substantial structural similarity with the 2-amino-4-oxo-1,4,7,8-tetrahydropteridin group on the substrate and may form the common motif for binding.

Further, the substrate dihydrofolate was titrated at several fixed concentrations of NSC133071 and NSC132277. When the resulting experimental curves were fit to the models for various types of inhibition, they showed equally good global fits to both competitive and linear mixed-type inhibition models (Fig S3A-B). However, based on visual assessment of the double-reciprocal Lineweaver–Burk plots, lines in which were seen intersecting on, or proximal to, the ordinate, the global fits shown are for the competitive displacement model (Fig. 5C and D). Further, Dixon analysis also showed that the lines intersect in the second quadrant, reinforcing the suggestion that the inhibition is competitive (data not shown). However, it should be noted that the long phenoxyalkyl and phenylalkyl substituents on the small molecules might give rise to some interaction with the protein that might lead to a slight perturbation in the maximum velocity observed, apart from its role in competitively displacing the substrate. This may lead to slight perturbation of the V_{max}, giving rise to the observed ambiguity in the non-linear fits. However, conclusive refutation of this model would require further experimentation. Moreover, an exact physical basis for this behavior might require detailed structural studies.

2.5. 1,3,5-Triazine-2,4-diamine analogs as uncompetitive inhibitors of NADPH binding

To understand the effect of 1,3,5-triazine-2,4-diamine derivatives on the cofactor NADPH binding, the latter was titrated at several fixed concentrations of the inhibitors. As before, the top four small molecules with the lowest K_{iapp} values, i.e., NSC120927, NSC132279, NSC133071 and NSC132277, were selected for this analysis. The resulting curves from the primary plot for all four small molecules, when globally fit to various types of inhibition models, showed the best fit to the model for uncompetitive inhibition (Fig. 6A–D). This yielded αK_i values, the equilibrium dissociation constant for the uncompetitive inhibitor, as specified in Table 3. These higher αK_i values, compared to the K_i values obtained from competition with substrate H_2F, show that the inhibitor binding site is fully formed only when the enzyme is bound to NADPH. It is worthwhile to point out that most reported inhibitors of *E. coli* DHFR show synergy with respect to NADPH binding [47]. However, it is evident from Fig. 6A–B that the fit of the primary curves to the global uncompetitive model deviates substantially from the experimental data points obtained at high inhibitor concentrations. This can be ascribed to the underestimation of inhibition at really high inhibitor concentrations by the model. To overcome this ambiguity by appropriate visual assessment, the resulting data were transformed and plotted as double-reciprocal LB plots. The right hand panels in Fig. 6A–D show parallel lines on the LB-plot. These confirm the fit of primary data to model for uncompetitive inhibition. The data on competition of the diaminotriazine derivatives with NADPH is strongly indicative of an ordered binding event whereby NADPH binding facilitates inhibitor binding.

2.6. Kinetics of NSC113909, a tight binder with poor inhibition

NSC113909, containing a fluorosulfonylphenylaminocarbonyl substitution at R2 on 1-phenyl-6,6-dimethyl-1,3,5-triazine-2,4-diamine ring, showed the unique behavior of tight-binding and average inhibition. To understand whether this molecule shows differential kinetics in its inhibition mechanism and the order of addition to the enzyme, detailed inhibition kinetics was carried out with this molecule too. Fig 7A shows the primary curves for H_2F titration at several different concentrations of NSC113909, fit to the model for competitive inhibition. Further, Fig 7B shows the double-reciprocal LB plot with lines intersecting on the ordinate. Likewise, Fig 7C shows the primary curves for NADPH titrations at several different concentrations of NSC113909 fit to the model for uncompetitive inhibition, and Fig 7D shows the double reciprocal LB plot, giving parallel lines. These patterns show that NSC113909 occupies the H_2F binding site and preferentially binds to the NADPH-bound form of the enzyme, mirroring the behavior shown by the best hits assessed in this study. However, the K_i value of 3.82 ± 0.43 μM for NSC113909 is much higher, indicative of poor inhibition of the enzyme (Table 3). As speculated earlier, this poorer inhibition might be because of two reasons: Partial charges from the carbonyl and amino group introduced as part of the linker might be incompatible with the NADPH-bound holo form of the enzyme or the planarity of the peptide bond due to electron pair delocalization might restrain the available degrees of freedom leading to unfavorable energy of interaction.

2.7. Discussion

E. coli DHFR follows a sequential mechanism, whereby product release is conditional upon binding of both substrates. Further, the substrates NADPH and H_2F can add to the enzyme randomly to form the Enzyme-NADPH-ternary complex. Understanding the mechanism of inhibition in a two-substrate reaction is a must for the success of a medicinal chemistry optimization exercise. Lack of understanding of the mechanism of a reaction may render a QSAR based drug-discovery program unproductive. Understanding the

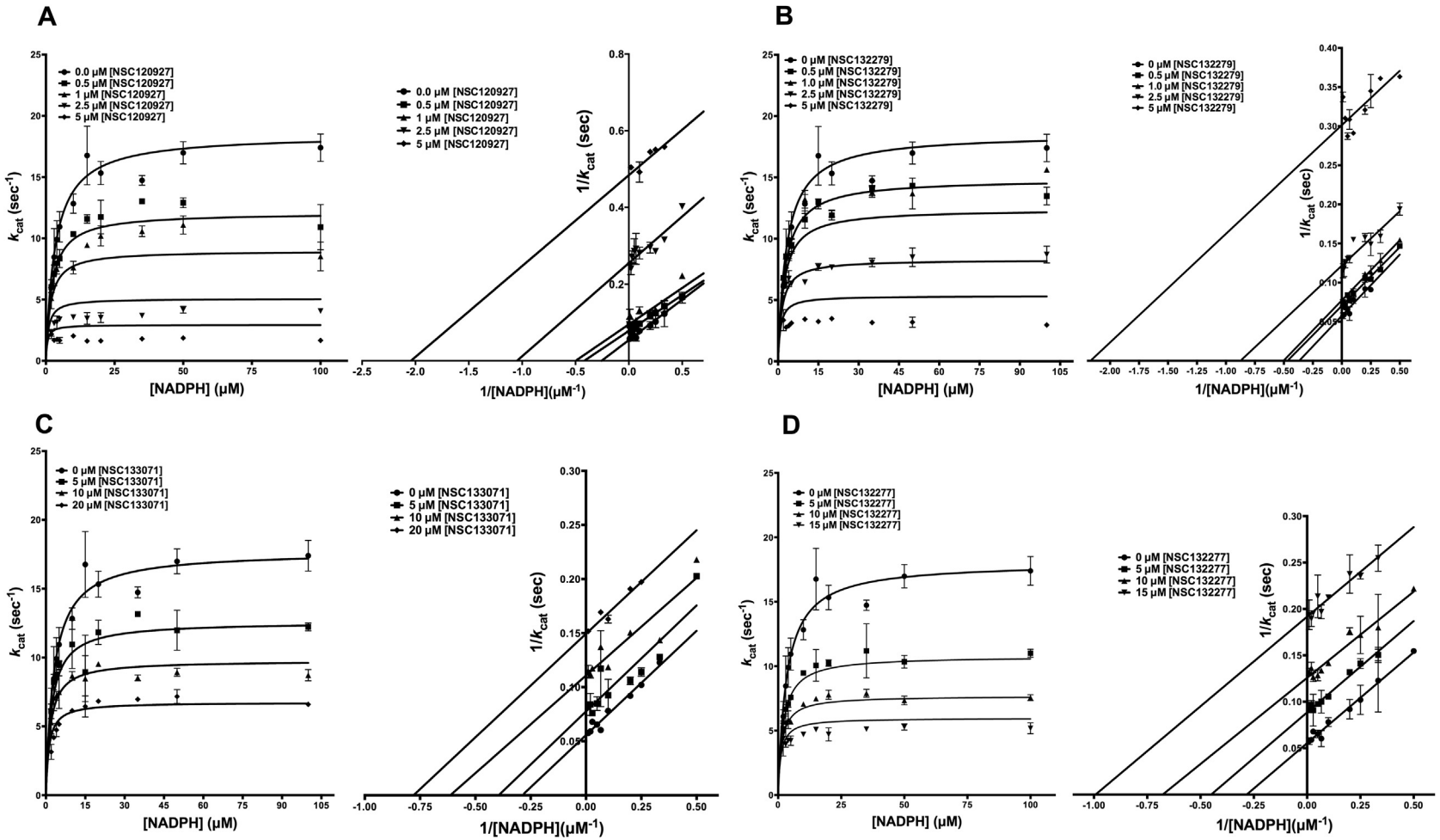

Fig. 6. Competition experiments of NSC120927, NSC132279, NSC133071 and NSC132277 against cofactor NADPH for *E. coli* DHFR. The plots show the fit of the primary data to the uncompetitive inhibition model and double reciprocal Lineweaver–Burk plot for NADPH titration at several fixed concentrations of (A) NSC120927, (B) NSC132279, (C) NSC133071 and (D) NSC132277. The y-axis shows the k_{cat} and k_{cat}^{-1} value and the x-axis shows the [NADPH] and 1/[NADPH] values for the primary and LB plot, respectively. The experimental data points were fit to the respective models using the non-linear curve-fitting algorithm of GraphPad Prism v 6.0e.

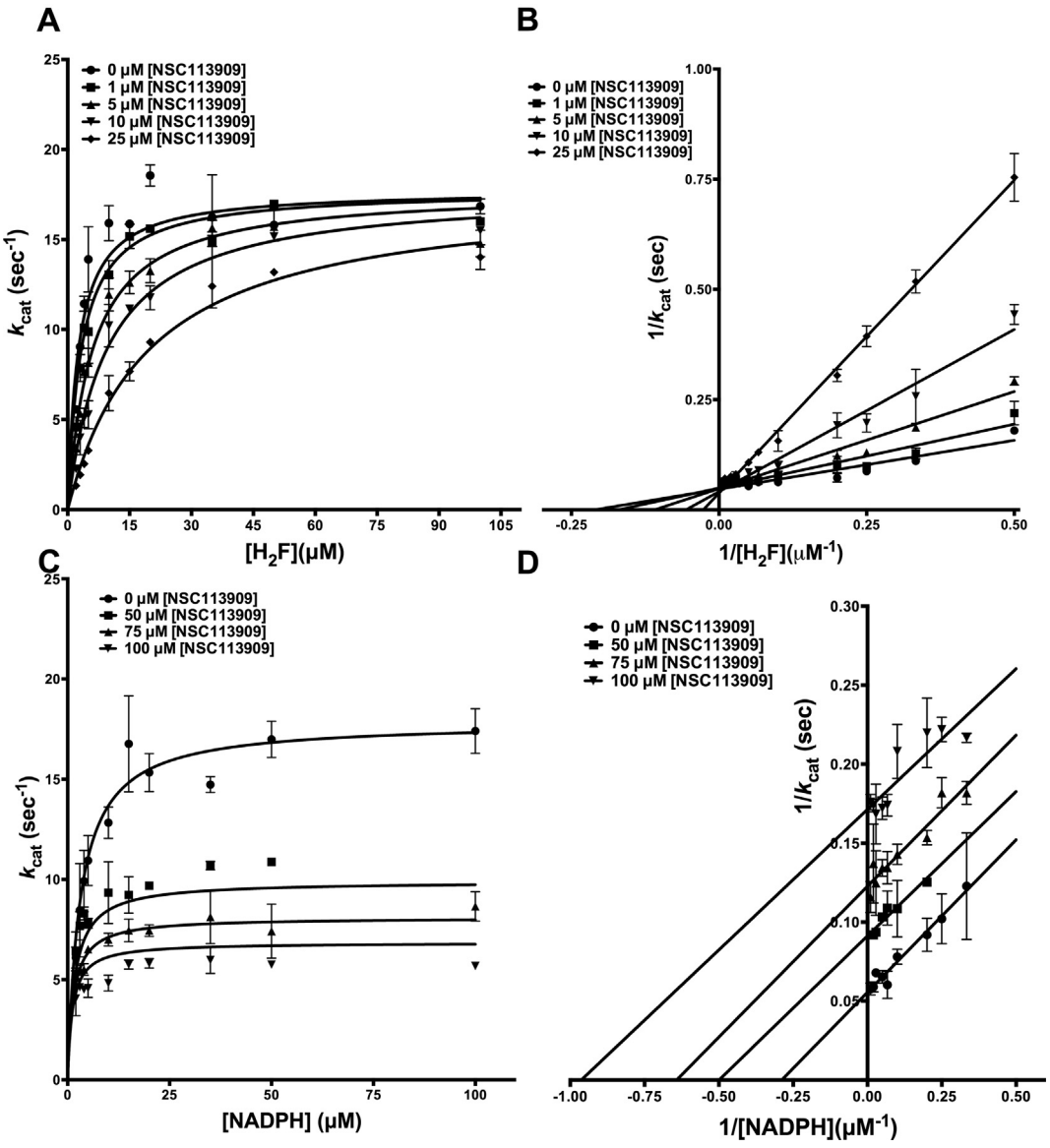

Fig. 7. Inhibition kinetics of NSC113909 for *E. coli* DHFR (A) Fit of the primary data to the competitive inhibition model for H_2F titration at several fixed concentrations of NSC113909. (B) Double reciprocal Lineweaver–Burk plot of H_2F titration at several fixed concentrations of NSC113909. (C) Fit of the primary data to the uncompetitive inhibition model for NADPH titration at several fixed concentrations of NSC113909. (D) Double reciprocal Lineweaver–Burk plot of NADPH titration at several fixed concentrations of NSC113909.

relationship between steady-state rate parameters and the specific form of the enzyme to which the inhibitor binds goes a long way towards ensuring the success of a drug-discovery program by narrowing the optimization of the SAR to achieve enrichment in binding/inhibition of the drug to that particular form of enzyme. Detailed mechanistic characterization of the top hits obtained in this study shows that the inhibitor molecules preferentially bind to the NADPH-bound binary form of the enzyme and are mostly competitive with the H_2F substrate. As pointed out by us in our previous study [17], it is desirable for an inhibitor to bind to the NADPH-bound form of *E. coli* DHFR given that *E. coli* cytoplasm has equal concentrations of both NADPH and NADP [48] and inhibition of the NADPH-bound, catalytically competent form of the enzyme would have maximum effect in enhancing the antibacterial activity of a compound.

The diaminotriazine family of compounds have been predominantly explored as inhibitors of eukaryotic DHFR, with the most notable application being inhibitors of *P. falciparum* DHFR [49,50]. Several studies have reported the application of diaminotriazine derivatives as drugs for wild type and drug-resistant mutants in *P. falciparum* [51–53]. However, to the best of our knowledge, there is a paucity of studies in which diaminotriazine compounds have been explored for their antibacterial activity, especially against gram-negative bacteria. This might be because of the poor inhibition of prokaryotic DHFRs by known diaminotriazine inhibitors. Structural analysis of various DHFR structures suggests that for a small-molecule to be a DHFR potent inhibitor, it must have a protonated N in the heterocyclic ring to enable the formation of a charge-mediated hydrogen bond with the enzyme. Furthermore, partial delocalization of the positive charge on the amino group adjacent to the protonated N contributes to the formation of an additional hydrogen bond, effectively increasing the binding affinity. An additional amino group at the para position relative to the protonated N group leads to additional hydrogen bonding. This in turn acts to increase the strength of protein–ligand interactions. In addition, the presence of hydrophobic substituents perpendicular

to the heterocyclic ring enables optimal polar and hydrophobic interactions with the enzyme [54]. The nanomolar inhibition constants of NSC132279 and NSC120927, the best inhibitors from our study against *E. coli* DHFR are encouraging from the perspective of utilizing diaminotriazines, a chemical scaffold that remains relatively unexplored for antibiotic discovery. It shows that, apart from the above-mentioned interactions pivotal for a small-molecule to function as an effective inhibitor, NSC120927 and NSC132279 make additional favorable interactions with the prokaryotic enzyme. Docking studies have indicated that the hydrophobic linker region and the terminal sulfonyl fluoride group makes several favorable interactions with the *E. coli* enzyme that can enable the development of this class of molecules as potent antibacterial agents. It should be pointed out here that nosocomial infections caused by multi-drug resistant *E. coli* are on the rise [55]. This clearly necessitates the discovery of newer scaffolds in antibiotic drug-discovery.

It should also be noted that none of the diaminotriazine compounds studied in this work displayed slow-onset of tight binding behavior. This is irrespective of the fact that two of the most potent hits had low nanomolar inhibition constants comparable to that shown by some of the well-known DHFR inhibitors. This is a unique observation, since it has been reported extensively in the literature that most, if not all, inhibitors of *E. coli* DHFR display slow-onset of tight binding [56]. In a previous study from our lab, we had shown that NSC309401, a 7-[(4-aminophenyl) methyl]-7H-pyrrolo [3,2-f] quinazoline-1,3-diamine, also shows slow-onset of tight binding inhibition of *E. coli* DHFR [17]. Further, we showed that the parent compound NSC339578, a 7H-pyrrolo [3,2-f] quinazoline-1,3-diamine, does not show slow-onset of inhibition in spite of being a tight binding inhibitor. This caused us to hypothesize that the nature of substitution on inhibitors of *E. coli* DHFR leads to the slow-onset behavior. In this study, none of the molecules showed slow-onset of inhibition irrespective of the nature of substituents. This suggests that the slow-onset of inhibition behavior might be a cooperative outcome of interactions made by the complete inhibitor molecule, rather than being an additive property of individual fragments.

Lamotrigine is a drug of the phenyltriazine class with inhibitory effects on voltage-sensitive sodium channels [57] that has also been shown to weakly inhibit mammalian dihydrofolate reductases [57,58]. It should be pointed out that lamotrigine is a 1,2,4-triazine-3,5-diamine, whereas the other compounds employed in this study are 1,3,5-triazine-2,4-diamine derivatives. This small-molecule was never explored for its potential as an inhibiting agent of prokaryotic DHFRs. In this study, we show for the first time that lamotrigine binds and inhibits *E. coli* DHFR with IC_{50} and K_{iapp} values of ~350 μM and ~15 μM, respectively. This finding opens up a whole new scaffold for antibacterial drug discovery and paves the way for next generation antibiotics to tackle the menace of increasing drug resistance in gram-negative bacteria.

2.8. Conclusions

In summary, this study is the first comprehensive binding and kinetic investigation of various derivatives of 1-phenyl-6,6-dimethyl-1,3,5-triazine-2,4-diamine to understand the effect of substitutions in their binding to and inhibition of *E. coli* DHFR. Further, this study throws light on the mechanism of inhibition by this family of compounds and shows that NSC120927 and NSC132279 are novel compounds with low nM inhibition constants against the *E. coli* DHFR. To the best of our knowledge, these molecules are the first ever nanomolar inhibitors of *E. coli* DHFR from this family of compounds and constitute potential antibiotic candidates.

3. Methods

3.1. Reagents

All reagents and chemicals, unless mentioned otherwise, were of high quality and were procured from Sigma–Aldrich Co., USA, Amresco, or Fisher Scientific. *E. coli* dihydrofolate reductase was provided by Prof. Eugene Shakhnovich, Harvard University. The small molecule NSC120927, NSC132279, NSC132277, NSC133071, NSC104129, NSC115928, NSC3074, NSC212229, NSC19732, NSC19745, NSC168184, NSC211137, NSC113909 and NSC117268 were provided by the Developmental Therapeutics Program (DTP) of the National Cancer Institute (NCI), National Institutes of Health (NIH). The small molecule CHEMBL597262 was kindly provided by Medicines for Malaria Venture (MMV) (http://www.mmv.org/malariabox). Dihydrofolate reductase assay kit (CS0340) was obtained from Sigma (Sigma–Aldrich, St. Louis, MO). Lamotrigine (L3791) was purchased from Sigma.

3.1.1. Binding studies using differential scanning fluorimetry, DSF

Binding of 16 small molecule compounds to *E. coli* DHFR was tested by differential scanning fluorimetry, DSF. The experiments were carried out following protocols reported in previous communications from our lab [13,17]. Briefly, the reactions were carried out in 20 μl reaction volumes in 96 well plates on the RealPlex quantitative PCR instrument (Eppendorf, NY, USA). The reaction mixture consisted of 100 mM HEPES pH 7.3 and 150 mM NaCl with 5× concentration of the reporter dye Sypro orange. Various compounds were tested for binding at a final concentration of 500 μM with 5 μM of *E. coli* DHFR. Compounds NSC132277 and NSC132279 failed to give signal at 500 μM and hence, the experiments were done at 10 μM.

The first derivatives of the thermal melt curves were fit to a Gaussian equation (Eq. (1)) for estimating the T_m (melting temperature) from the observed intensity of fluorescence, I.

$$f(x,\mu,\sigma) = \left(1\Big/\sigma\sqrt{2\pi}\right)e^{(-0.5((x-\mu)/\sigma))\hat{2}} \quad (1)$$

Here, μ is the mean of the Gaussian distribution, σ is the standard deviation and σ^2 is the variance. Thermodynamic parameters and apparent dissociation constants (K_{Dapp}) were estimated as specified in the previous literature [13].

3.1.2. Dihydrofolate reductase assay

DHFR was assayed as previously reported [17]. Briefly, the formation of NADP was monitored by the decrease in absorbance at 340 nm for 100 s. The amount of product formed was computed from the slopes of time-course measurements using a molar extinction coefficient (ε) of 6.2 × 10^3 M^{-1} cm^{-1} for β-NADPH at 340 nm [59]. The non-enzymatic hydrolysis of NADPH was normalized. Assays were initiated with the addition of enzyme to the sample cuvette after zeroing the absorbance reading with respect to the reference cuvette. The initial velocities, where product formation was less than 5%, were measured for reaction mixtures containing 100 mM HEPES pH 7.3 at room temperature (~22° C).

All the measurements were performed in duplicate, and the error values indicated are standard errors (S.E.). The concentration of *E. coli* DHFR used was 16.7 nM and was estimated by the method of velocity–titration curves as previously reported [17]. Unless mentioned otherwise, all the data were fit using non-linear curve fitting subroutines of GraphPad Prism, version 4.0 (GraphPad Software, Inc., San Diego, CA).

3.1.3. Inhibition kinetics

14 compounds with varied substitutions of diaminotriazine were assessed for their inhibitory effect on the NADPH oxidizing ability of *E. coli* DHFR. Both the dose-dependence of inhibition and affinity of the inhibitor for the enzyme were computed by experimental IC_{50} determination and competition assays to determine its K_i. IC_{50} determination assays were carried out in 100 mM HEPES pH 7.3, 60 μM NADPH, 50 μM H_2F and variable concentration of each inhibitor. The enzyme concentration was as specified above. The curves were fit to equation (2),

$$y = 100\%/[1 + (I/IC_{50})] \quad (2)$$

where, I is the inhibitor concentration, and y is the percentage of activity.

Furthermore, K_i^{app} values were computed from the IC_{50} curves by fitting them to the quadratic Morrison equation (3) assuming competitive inhibition.

$$v_i/v_0 = 1 - \left(\left([E]_T + [I]_T + K_i^{app} \right) - \sqrt{\left([E]_T + [I]_T + K_i^{app} \right)^2 - 4[E]_T[I]_T} \right) \Big/ 2[E]_T \quad (3)$$

where, v_i represents velocity in the presence of inhibitor, v_0 represents velocity in the absence of inhibitor, $[E]_T$ represents total enzyme, $[I]_T$ represents total inhibitor and K_i^{app} represents apparent K_i.

Experimental K_i value determinations were carried out by titrating the substrates H_2F and NADPH, around their respective K_m values at various fixed concentrations of the inhibitors around their K_{iapp} values. The substrate or cofactor that is not varied is kept at a fixed saturating concentration greater than 10 times their respective K_m values. The resulting [substrate] vs. velocity curves were fit to models of competitive inhibition (equation (4)), non-competitive inhibition (equation (5)), uncompetitive inhibition (equation (6)) and linear mixed-type inhibition (equation (7)) in order to discriminate between the different types of inhibition and to estimate the various inhibition constants (K_i).

Competitive:

$$v = V_{max}[S]/\{K_m(1 + [I]/K_i) + [S]\} \quad (4)$$

Non-competitive:

$$v = V_{max}[S]/\{K_m(1 + [I]/K_i) + [S](1 + [I]/K_i)\} \quad (5)$$

Uncompetitive:

$$v = V_{max}[S]/\{K_m + [S](1 + [I]/K_i)\} \quad (6)$$

Linear Mixed-type:

$$v = V_{max\_app}[S]/(K_{m\_app} + [S]) \quad (7)$$

$$V_{max\_app} = V_{max}/(1 + I/(\alpha K_i)) \quad (8)$$

$$K_{m\_app} = K_m(1 + I/K_i)/(1 + I/(\alpha Ki)) \quad (9)$$

where, v is the velocity of the reaction, V_{max} is the maximum velocity, [S] is the substrate concentration, and [I] is the inhibitor concentration. K_m is the Michaelis–Menten constant, and K_i is the inhibition constant. Visual assessment of the type of inhibition was undertaken by plotting the double reciprocal Lineweaver–Burk plot from experimental data points constituting the primary plot.

3.1.4. QSAR analysis

The various physicochemical properties of the small molecules employed in this study were computed from ChemMine tools employing OpenBabel and Joelib descriptors [60] and ChemBioDraw 14.0. Pearson's correlation analysis was carried out individually on each parameter against the obtained inhibition constants and the equation was derived by linear regression with GraphPad Prism, version 4.0. Genetic algorithm analysis was carried out using the opensource QSAR model development algorithm provided by Nanobridges.

3.1.5. Template based docking of small molecules

In order to find the interacting pose of the predicted small molecules with DHFR, template based docking was performed using the structure of DHFR in complex with folate (PDB_ID: 1RX7) [43] as the template. This was achieved by using the known interacting pose of folate with DHFR as the template and aligning the small molecules to it. To do so, initially we generated 200 different conformers for each of the predicted ligands using the open source chemoinformatics software RDKit [61]. Next, LIGSIFT [44] was used to perform a structural alignment of each of the conformers to folate's structure obtained in its crystal structure with DHFR. Finally, the best conformer for each case with the most significant P-value was chosen and superposed on folate. Both shape and chemical similarities between the two molecules were used to produce the alignments, and in cases where there were no significant alignments, only shape similarity was used to align the two molecules. The initial 3D conformation of each of the predicted ligands was obtained from PubChem [62], and Open Babel [63] was used for converting different file formats (e.g. SDF to MOL2 format).

Author contributions

BS conceived of the study, participated in its design, carried out the experiments, analyzed and interpreted the results, and drafted the manuscript. ST-N performed the docking studies, and was involved in drafting and critically reviewing the manuscript. JS conceived of the study, participated in its design and coordination, provided appropriate resources, helped analyze the data, and was involved in drafting and critically reviewing the manuscript. All authors read and approved the final manuscript.

Acknowledgments

This project was funded by GM-37408 and GM-48835 of the Division of General Medical Sciences of the NIH. The authors wish to thank Prof. Eugene Shakhnovich, Harvard University for providing purified *E. coli* DHFR protein. We would also like to thank the Developmental Therapeutics Program of the National Cancer Institute for providing the small molecules used in this study.

Appendix A. Supplementary data

Supplementary data related to this article can be found at http://dx.doi.org/10.1016/j.ejmech.2015.08.021.

References

[1] H. Nikaido, Multidrug efflux pumps of gram-negative bacteria, J. Bacteriol. 178 (1996) 5853–5859.
[2] D.L. Paterson, Resistance in gram-negative bacteria: Enterobacteriaceae, Am. J. Infect. Control 34 (2006) S20–S28 discussion S64–73.
[3] M. Vaara, Antibiotic-supersusceptible mutants of *Escherichia coli* and *Salmonella typhimurium*, Antimicrob. Agents Chemother. 37 (1993) 2255–2260.
[4] F. Daxboeck, T. Budic, O. Assadian, M. Reich, W. Koller, Economic burden associated with multi-resistant Gram-negative organisms compared with that for methicillin-resistant *Staphylococcus aureus* in a university teaching hospital, J. Hosp. Infect. 62 (2006) 214–218.
[5] R.J. Fair, Y. Tor, Antibiotics and bacterial resistance in the 21st century, Perspect. Med. Chem. 6 (2014) 25–64.
[6] S. Vasoo, J.N. Barreto, P.K. Tosh, Emerging issues in gram-negative bacterial resistance: an update for the practicing clinician, Mayo Clin. Proc. 90 (2015) 395–403.
[7] R.L. Finley, P. Collignon, D.G. Larsson, S.A. McEwen, X.Z. Li, W.H. Gaze, R. Reid-Smith, M. Timinouni, D.W. Graham, E. Topp, The scourge of antibiotic resistance: the important role of the environment, Clin. Infect. Dis. Off. Publ. Infect. Dis. Soc. Am. 57 (2013) 704–710.
[8] P.M. Hawkey, A.M. Jones, The changing epidemiology of resistance, J. Antimicrob. Chemother. 64 (Suppl. 1) (2009) i3–10.
[9] M.E. Ibrahim, N.E. Bilal, M.E. Hamid, Increased multi-drug resistant *Escherichia coli* from hospitals in Khartoum state, Sudan, Afr. Health Sci. 12 (2012) 368–375.
[10] I. Schlackow, N. Stoesser, A.S. Walker, D.W. Crook, T.E. Peto, D.H. Wyllie, Infections in Oxfordshire Research Database, T, Increasing incidence of Escherichia coli bacteraemia is driven by an increase in antibiotic-resistant isolates: electronic database study in Oxfordshire 1999–2011, J. Antimicrob. Chemother. 67 (2012) 1514–1524.
[11] S.K. Swami, J.T. Liesinger, N. Shah, L.M. Baddour, R. Banerjee, Incidence of antibiotic-resistant *Escherichia coli* bacteriuria according to age and location of onset: a population-based study from Olmsted County, Minnesota, Mayo Clin. Proc. 87 (2012) 753–759.
[12] B.I. Schweitzer, A.P. Dicker, J.R. Bertino, Dihydrofolate reductase as a therapeutic target, FASEB J. Off. Publ. Fed. Am. Soc. Exp. Biol. 4 (1990) 2441–2452.
[13] B. Srinivasan, H. Zhou, J. Kubanek, J. Skolnick, Experimental validation of FINDSITE(comb) virtual ligand screening results for eight proteins yields novel nanomolar and micromolar binders, J. Cheminformatics 6 (2014) 16.
[14] J.Y. Fukunaga, C. Hansch, E.E. Steller, Inhibition of dihydrofolate reductase. Structure-activity correlations of quinazolines, J. Med. Chem. 19 (1976) 605–611.
[15] L.F. Kuyper, D.P. Baccanari, M.L. Jones, R.N. Hunter, R.L. Tansik, S.S. Joyner, C.M. Boytos, S.K. Rudolph, V. Knick, H.R. Wilson, J.M. Caddell, H.S. Friedman, J.C. Comley, J.N. Stables, High-affinity inhibitors of dihydrofolate reductase: antimicrobial and anticancer activities of 7,8-dialkyl-1,3-diaminopyrrolo[3,2-f]quinazolines with small molecular size, J. Med. Chem. 39 (1996) 892–903.
[16] A. Rosowsky, J.B. Hynes, S.F. Queener, Structure-activity and structure-selectivity studies on diaminoquinazolines and other inhibitors of *Pneumocystis carinii* and *Toxoplasma gondii* dihydrofolate reductase, Antimicrob. Agents Chemother. 39 (1995) 79–86.
[17] B. Srinivasan, J. Skolnick, Insights into the slow-onset tight-binding inhibition of *Escherichia coli* dihydrofolate reductase: detailed mechanistic characterization of pyrrolo [3,2-f] quinazoline-1,3-diamine and its derivatives as novel tight-binding inhibitors, FEBS J. 282 (10) (2015) 1922–1938.
[18] B.A. Srinivasan, Jeffrey Skolnick, Hongyi Zhou, Molecules with Potent DHFR Binding Affinity and Antibacterial Activity, Georgia Tech Research Corporation, (Atlanta, GA, US), United States, 2014.
[19] R.L. Li, M. Poe, Quantitative structure-activity relationships for the inhibition of *Escherichia coli* dihydrofolate reductase by 5-(substituted benzyl)-2,4-diaminopyrimidines, J. Med. Chem. 31 (1988) 366–370.
[20] D.P. Baccanari, S. Daluge, R.W. King, Inhibition of dihydrofolate reductase: effect of reduced nicotinamide adenine dinucleotide phosphate on the selectivity and affinity of diaminobenzylpyrimidines, Biochemistry 21 (1982) 5068–5075.
[21] L.C. Chio, S.F. Queener, Identification of highly potent and selective inhibitors of *Toxoplasma gondii* dihydrofolate reductase, Antimicrob. Agents Chemother. 37 (1993) 1914–1923.
[22] C. Hansch, R. Li, J.M. Blaney, R. Langridge, Comparison of the inhibition of *Escherichia coli* and *Lactobacillus casei* dihydrofolate reductase by 2,4-diamino-5-(substituted-benzyl)pyrimidines: quantitative structure-activity relationships, X-ray crystallography, and computer graphics in structure-activity analysis, J. Med. Chem. 25 (1982) 777–784.
[23] J.W. Williams, J.F. Morrison, R.G. Duggleby, Methotrexate, a high-affinity pseudosubstrate of dihydrofolate reductase, Biochemistry 18 (1979) 2567–2573.
[24] J.M. Blaney, C. H, C. Silipo, A. Vittoria, Structure-activity relationships of dihydrofolate reductase inhibitors, Chem. Rev. 84 (1984) 333–407.
[25] H.A. Akio Ohsawa, Hidefumi Ohnishi, Hiroshi Igeta, 1,2,3-Triazine, J. Chem. Soc. Chem. Commun. (22) (1981), 1174-1174.
[26] M.J. Leach, M.G. Baxter, M.A. Critchley, Neurochemical and behavioral aspects of lamotrigine, Epilepsia 32 (Suppl. 2) (1991) S4–S8.
[27] D.A. Fidock, T. Nomura, T.E. Wellems, Cycloguanil and its parent compound proguanil demonstrate distinct activities against *Plasmodium falciparum* malaria parasites transformed with human dihydrofolate reductase, Mol. Pharmacol. 54 (1998) 1140–1147.
[28] Y. Yuthavong, B. Tarnchompoo, T. Vilaivan, P. Chitnumsub, S. Kamchonwongpaisan, S.A. Charman, D.N. McLennan, K.L. White, L. Vivas, E. Bongard, C. Thongphanchang, S. Taweechai, J. Vanichtanankul, R. Rattanajak, U. Arwon, P. Fantauzzi, J. Yuvaniyama, W.N. Charman, D. Matthews, Malarial dihydrofolate reductase as a paradigm for drug development against a resistance-compromised target, Proc. Natl. Acad. Sci. U. S. A. 109 (2012) 16823–16828.
[29] R.G. Booth, C.D. Selassie, C. Hansch, D.V. Santi, Quantitative structure-activity relationship of triazine-antifolate inhibition of Leishmania dihydrofolate reductase and cell growth, J. Med. Chem. 30 (1987) 1218–1224.
[30] E.A. Coats, C.S. Genther, S.W. Dietrich, Z.R. Guo, C. Hansch, Comparison of the inhibition of methotrexate-sensitive and -resistant *Lactobacillus casei* cell cultures with purified *Lactobacillus casei* dihydrofolate reductase by 4,6-diamino-1,2-dihydro-2,2-dimethyl-1-(3-substituted-phenyl)-s-triazines. Use of quantitative structure-activity relationships in making inferences about the mechanism of resistance and the structure of the enzyme is situ compared with the enzyme in vitro, J. Med. Chem. 24 (1981) 1422–1429.
[31] C. Hansch, S.W. Dietrich, J.Y. Fukunaga, Inhibition of bovine and rat liver dihydrofolate reductase by 4,6-diamino-1,2-dihydro-2,2-dimethyl-1-(4-substituted-phenyl)-s-triazines, J. Med. Chem. 24 (1981) 544–549.
[32] C. Hansch, B.A. Hathaway, Z.R. Guo, C.D. Selassie, S.W. Dietrich, J.M. Blaney, R. Langridge, K.W. Volz, B.T. Kaufman, Crystallography, quantitative structure-activity relationships, and molecular graphics in a comparative analysis of the inhibition of dihydrofolate reductase from chicken liver and *Lactobacillus casei* by 4,6-diamino-1,2-dihydro-2,2-dimethyl-1-(substituted-phenyl)-s-triazine s, J. Med. Chem. 27 (1984) 129–143.
[33] K.H. Kim, S.W. Dietrich, C. Hansch, B.J. Dolnick, J.R. Bertino, Inhibition of dihydrofolate reductase. 3. 4.6-Diamino-1,2-dihydro-2,2-dimethyl-1-(2-substituted-phenyl)-s-triazine inhibition of bovine liver and mouse tumor enzymes, J. Med. Chem. 23 (1980) 1248–1251.
[34] C.K. Marlowe, C.D. Selassie, D.V. Santi, Quantitative structure-activity relationships of the inhibition of *Pneumocystis carinii* dihydrofolate reductase by 4,6-diamino-1,2-dihydro-2,2-dimethyl-1-(X-phenyl)-s-triazines, J. Med. Chem. 38 (1995) 967–972.
[35] E.F.F. da Cunha, T.C. R., E.R. Maia, R.B. de Alencastra, The search for new DHFR inhibitors: a review of patents, January 2001–February 2005, Expert Opin. Ther. Pat. 15 (2005) 1–20.
[36] B.A. Hathaway, Z.R. Guo, C. Hansch, T.J. Delcamp, S.S. Susten, J.H. Freisheim, Inhibition of human dihydrofolate reductase by 4,6-diamino-1,2-dihydro-2,2-dimethyl-1-(substituted-phenyl)-s-triazine s. A quantitative structure-activity relationship analysis, J. Med. Chem. 27 (1984) 144–149.
[37] A.C. Lele, A. R., M.K. Ray, M.G.R. Rajan, M.S. Degani, Design and synthesis of diaminotriazines as anti-tuberculosis DHFR inhibitors, Curr. Res. Drug Discov. 1 (2014), 45–40.
[38] C.D. Selassie, C.D. Strong, C. Hansch, T.J. Delcamp, J.H. Freisheim, T.A. Khwaja, Comparison of triazines as inhibitors of L1210 dihydrofolate reductase and of L1210 cells sensitive and resistant to methotrexate, Cancer Res. 46 (1986) 744–756.
[39] D.P. Jacobus, G.A. Schiehser, H.M. Shieh, N.P. Jensen, J. Terpinski. Biguanide and dihydrotriazine derivatives, Google Patents (2007).
[40] P. Singla, V. Luxami, K. Paul, Triazine-benzimidazole hybrids: anticancer activity, DNA interaction and dihydrofolate reductase inhibitors, Bioorg. Med. Chem. 23 (2015) 1691–1700.
[41] S.I.K. Deepak Kumar, Prija Ponnan, Diwan S. Rawat, Triazine–pyrimidine based molecular hybrids: synthesis, docking studies and evaluation of anti-malarial activity, New J. Chem. 38 (2014) 5087–5095.
[42] K. Roy, I. Mitra, On various metrics used for validation of predictive QSAR models with applications in virtual screening and focused library design, Comb. Chem. High Throughput Screen. 14 (2011) 450–474.
[43] M.R. Sawaya, J. Kraut, Loop and subdomain movements in the mechanism of *Escherichia coli* dihydrofolate reductase: crystallographic evidence, Biochemistry 36 (1997) 586–603.
[44] A. Roy, J. Skolnick, LIGSIFT: an open-source tool for ligand structural alignment and virtual screening, Bioinformatics 31 (2015) 539–544.
[45] B.R. Brooks, R.E. Bruccoleri, B.D. Olafson, D.J. States, S. Swaminathan, M. Karplus, CHARMM: a program for macromolecular energy, minimization, and dynamics calculations, J. Comp. Chem. 4 (1983) 187–217.
[46] R. Taylor, O. Kennard, Crystallographic evidence for the existence of CHO, CHN and CHCl hydrogen bonds, J. Am. Chem. Soc. 104 (1982) 5063–5070.
[47] S.R. Stone, J.F. Morrison, Mechanism of inhibition of dihydrofolate reductases from bacterial and vertebrate sources by various classes of folate analogues, Biochim. Biophys. Acta 869 (1986) 275–285.
[48] J.R. Appleman, W.A. Beard, T.J. Delcamp, N.J. Prendergast, J.H. Freisheim, R.L. Blakley, Unusual transient- and steady-state kinetic behavior is predicted by the kinetic scheme operational for recombinant human dihydrofolate reductase, J. Biol. Chem. 265 (1990) 2740–2748.
[49] N.P. Jensen, A.L. Ager, R.A. Bliss, C.J. Canfield, B.M. Kotecka, K.H. Rieckmann, J. Terpinski, D.P. Jacobus, Phenoxypropoxybiguanides, prodrugs of DHFR-inhibiting diaminotriazine antimalarials, J. Med. Chem. 44 (2001) 3925–3931.
[50] A. Nzila, Inhibitors of de novo folate enzymes in *Plasmodium falciparum*, Drug Discov. Today 11 (2006) 939–944.

[51] D.S. Peterson, W.K. Milhous, T.E. Wellems, Molecular basis of differential resistance to cycloguanil and pyrimethamine in *Plasmodium falciparum* malaria, Proc. Natl. Acad. Sci. U. S. A. 87 (1990) 3018–3022.
[52] P. Maitarad, S. Kamchonwongpaisan, J. Vanichtanankul, T. Vilaivan, Y. Yuthavong, S. Hannongbua, Interactions between cycloguanil derivatives and wild type and resistance-associated mutant *Plasmodium falciparum* dihydrofolate reductases, J. Comput. Aided Mol. Des. 23 (2009) 241–252.
[53] S.C. Basak, D. Mills, Quantitative structure-activity relationships for cycloguanil analogs as PfDHFR inhibitors using mathematical molecular descriptors, SAR QSAR Environ. Res. 21 (2010) 215–229.
[54] M. Xiang, Synthesis and Bioactivity Study of 4,6-diamino-1,3,5-triazines, in: Department of Pharmacy, National University of Singapore, Singapore, 2006, pp. 41–42.
[55] A.J. Mathers, G. Peirano, J.D. Pitout, The role of epidemic resistance plasmids and international high-risk clones in the spread of multidrug-resistant Enterobacteriaceae, Clin. Microbiol. Rev. 28 (2015) 565–591.
[56] S.R. Stone, J.A. Montgomery, J.F. Morrison, Inhibition of dihydrofolate reductase from bacterial and vertebrate sources by folate, aminopterin, methotrexate and their 5-deaza analogues, Biochem. Pharmacol. 33 (1984) 175–179.
[57] X. Ma, T.Y. Poon, P.T. Wong, W.K. Chui, Synthesis and in vitro evaluation of 2,4-diamino-1,3,5-triazine derivatives as neuronal voltage-gated sodium channel blockers, Bioorg. Med. Chem. Lett. 19 (2009) 5644–5647.
[58] K.D. Laxer, Guidelines for treating epilepsy in the age of felbamate, vigabatrin, lamotrigine, and gabapentin, West. J. Med. 161 (1994) 309–314.
[59] B.L. Horecker, A. Kornberg, The extinction coefficients of the reduced band of pyridine nucleotides, J. Biol. Chem. 175 (1948) 385–390.
[60] T.W. Backman, Y. Cao, T. Girke, ChemMine tools: an online service for analyzing and clustering small molecules, Nucleic Acids Res. 39 (2011) W486–W491.
[61] G. Landrum. RDKit: Open-source cheminformatics.
[62] Q. Li, T. Cheng, Y. Wang, S.H. Bryant, PubChem as a public resource for drug discovery, Drug Discov. Today 15 (2010) 1052–1057.
[63] N.M. O'Boyle, M. Banck, C.A. James, C. Morley, T. Vandermeersch, G.R. Hutchison, Open Babel: an open chemical toolbox, J. Cheminformatics 3 (2011) 33.
[64] J. Stone, An efficient library for parallel Ray tracing and animation, in: Computer Science, University of Missouri, 1998.
[65] W. Humphrey, A. Dalke, K. Schulten, VMD: visual molecular dynamics, J. Mol. Graph. 14 (1996) 33–38, 27–38.